NANO LETTERS

pubs.acs.org/NanoLett Letter

Incorporating the Nanoscale Encapsulation Concept from Liquid Electrolytes into Solid-State Lithium–Sulfur Batteries

Xin Gao, Xueli Zheng, Jingyang Wang, Zewen Zhang, Xin Xiao, Jiayu Wan, Yusheng Ye, Lien-Yang Chou, Hiang Kwee Lee, Jiangyan Wang, Rafael A. Vilá, Yufei Yang, Pu Zhang, Lin-Wang Wang, and Yi Cui*

Cite This: https://dx.doi.org/10.1021/acs.nanolett.0c02033 Read Online

ACCESS | Metrics & More | Article Recommendations | Supporting Information

ABSTRACT: Solid-state Li–S batteries are attractive due to their high energy density and safety. However, it is unclear whether the concepts from liquid electrolytes are applicable in the solid state to improve battery performance. Here, we demonstrate that the nanoscale encapsulation concept based on $Li_2S@TiS_2$ core–shell particles, originally developed in liquid electrolytes, is effective in solid polymer electrolytes. Using in situ optical cell and sulfur K-edge X-ray absorption, we find that polysulfides form and are well-trapped inside individual particles by the nanoscale TiS_2 encapsulation. This TiS_2 encapsulation layer also functions to catalyze the oxidation reaction of Li_2S to sulfur, even in solid-state electrolytes, proven by both experiments and density functional theory calculations. A high cell-level specific energy of 427 W·h·kg^{-1} is achieved by integrating the $Li_2S@TiS_2$ cathode with a poly(ethylene oxide)-based electrolyte and a lithium metal anode. This study points to the fruitful direction of borrowing concepts from liquid electrolytes into solid-state batteries.

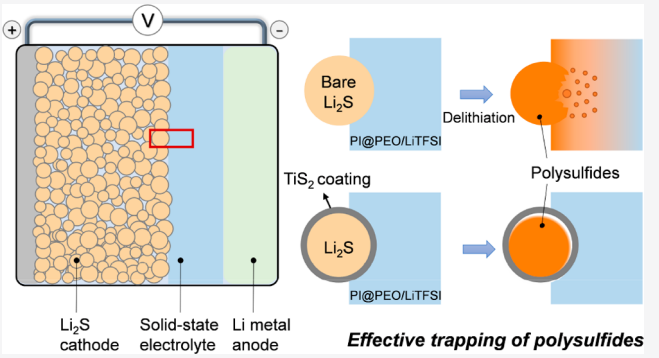

KEYWORDS: *Li–S batteries, solid-state electrolytes, nanoscale encapsulation, polysulfide entrapment, in situ optical cell*

Rapid developments of electric vehicles and portable electronics have triggered the quest for new battery technologies with energy densities greater than those of current lithium-ion batteries.[1,2] Lithium–sulfur (Li–S) batteries are considered as the most promising candidate because of their low cost and high theoretical energy density (2500 W·h·kg^{-1}), a 5-fold increase compared to that of traditional lithium-ion batteries.[3−5] In the past, most Li–S related battery research was done in liquid electrolytes. The practical applications of Li–S batteries are found to be hampered by the low electronic and lithium-ion conductivity of sulfur and lithium sulfide (Li_2S), polysulfide shuttling, and poor stability of lithium metal anodes.[6−9] These limitations result in poor sulfur utilization, fast capacity fading, and safety issues. Significant research on Li–S batteries (in liquid electrolytes) has been devoted to addressing these issues, the most successful of which have been design of nanostructured hosts,[10,11] encapsulation of sulfur species,[12,13] separator modification,[14,15] and formation of a uniform solid electrolyte interphase (SEI).[16]

Recently, there is a new direction to address Li–S chemistry by replacing flammable liquid electrolytes with solid-state electrolytes.[17−20] There are two main types of solid electrolytes to be considered: inorganic ceramics and organic polymers. Although inorganic solid electrolytes have the highest lithium-ion conductivity at room temperature,[21−24] their high mass density (e.g., $Li_7La_3Zr_2O_{12}$, 5.2 g·cm^{-3}) and brittle nature present a challenge for applications.[25,26] In contrast, solid polymer electrolytes (SPEs) can balance a moderate lithium-ion conductivity with a lower mass density (~1 g·cm^{-3}), improved mechanical flexibility, and ease of processing.[27,28] Many studies show the lithium-ion conductivity of SPEs is improved by adding inorganic fillers such as silicon oxide,[29] titanium oxide,[30] zirconium oxide,[18] and lithium-ion conducting ceramics.[31,32] Recently, an ultrathin polymer–polymer composite electrolyte (8.6 μm) with high ion conductivity of 2.3×10^{-4} S·cm^{-1} at 30 °C was developed using the concept of vertical channels.[33] Fireproof and lightweight SPEs are further developed to improve the safety of lithium batteries.[34] These improvements drive the research field toward achieving high energy density and safe all-solid-state Li–S batteries (ASSLSBs). However, several intrinsic issues of conversion

Received: May 12, 2020
Revised: June 4, 2020
Published: June 9, 2020

chemistry between sulfur and Li_2S in ASSLSBs still need to be addressed, such as the insulating properties of sulfur and Li_2S and interfacial parasitic reactions toward the anode side.[35] Particularly, we want to point out that the hypothesis that SPEs suppress polysulfide dissolution is found to be incorrect, and recent studies show that significant polysulfide dissolution occurs in SPEs.[36−38]

Here, we propose that some of the material design improvements originally developed for liquid electrolytes can be incorporated to solid electrolytes with excellent outcomes. However, thus far, there are very few studies exploring those concepts in solid-state Li−S battery systems. Some recent attempts are listed here. Sulfur was infiltrated in porous carbon hosts to improve the electronic conductivity of cathodes and therefore to enhance the performance of ASSLSBs.[31,39] Different lithium salts have been incorporated into SPEs to regulate the interfacial chemistry of the lithium metal anode, thus creating a compact and highly conductive SEI.[40−42] Unfortunately, solid-polymer-based ASSLSBs still fail to reach satisfactory performance because an effective strategy to avoid polysulfide dissolving into SPEs is still missing.

Nanoscale encapsulation of sulfur cathodes has been demonstrated in liquid electrolytes,[12,13,43,44] although it is unknown whether the encapsulation concept is feasible in solid-polymer-based ASSLSBs. Indeed, the encapsulation concept has not yet been explored in the solid electrolyte Li−S system. In this study, we apply the concept of nanoscale encapsulation for the first time in solid-polymer-based ASSLSBs. We use a thin (∼20 nm) layered titanium disulfide (TiS_2) encapsulation to inhibit polysulfide dissolution into SPEs in all-solid-state Li_2S−Li batteries (Figure 1a). Li_2S cathodes are chosen because Li_2S is already in the expanded state (compared to sulfur), which prevents fracture of the encapsulation layer by volume expansion. In addition, Li_2S cathodes are compatible with anode-free cells.[45] From previous studies in liquid electrolytes, TiS_2 encapsulation efficiently prevents polysulfide dissolution because of a strong binding with Li_2S/Li_2S_x species.[46] We hypothesize that TiS_2 encapsulation can also prevent polysulfide dissolution into SPEs because the strong binding of Li_2S/Li_2S_x species to TiS_2 applies even in the absence of liquid electrolytes. In comparison, for Li_2S cathode without TiS_2 encapsulation (bare Li_2S), intermediate polysulfides form and dissolve into SPEs (Figure 1b,c). We hypothesize the designed TiS_2-encapsulated Li_2S ($Li_2S@TiS_2$) cathode can facilitate the transformation of Li_2S into S in solid electrolytes, as it is the case in liquid electrolytes. We demonstrated that a high cell-level energy density of 427 $W{\cdot}h{\cdot}kg^{-1}$ (including the mass of the anode, cathode, and solid-state electrolyte, but excluding the current collector and packaging) is achieved by integrating $Li_2S@TiS_2$ cathodes with ultrathin poly(ethylene oxide) (PEO)-based solid-state electrolyte (10−20 μm, Supporting Information Figure S1) and a lithium metal anode. We provide proof in this work that nanoscale encapsulation is effective for Li−S batteries in the solid-state electrolyte system. There exists catalytic Li_2S oxidation for ASSLSBs while preventing polysulfide dissolution by nanoscale encapsulation with TiS_2. We believe that bringing material design concepts from liquid electrolytes into solid-state Li−S batteries represents a new and exciting direction.

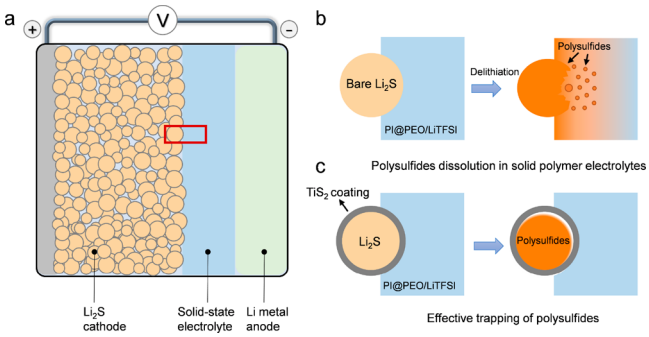

Figure 1. Design of encapsulated Li_2S cathodes for solid polymer based ASSLSBs. (a) Schematic of the ASSLSB architecture comprising lithium metal anodes, nanoporous polyimide (PI) film filled with PEO/lithium bis(trifluoromethanesulfonyl)imide (PI@PEO/LiTFSI) solid electrolytes, and Li_2S composite cathodes. Zoomed-in schemes of the red rectangle in (a) to depict the interface between the solid-state electrolyte and the cathode during delithiation process for (b) bare Li_2S cathode and (c) $Li_2S@TiS_2$ cathode. Bare Li_2S particles undergo polysulfide dissolution upon delithiation, resulting in rapid capacity decay and low Coulombic efficiency. $Li_2S@TiS_2$ core−shell structure provides a structurally intact shell for effective trapping of polysulfides, thereby avoiding polysulfide dissolution into SPEs. Light yellow, Li_2S particles; orange, polysulfide; gray shell, TiS_2 coating.

Encapsulation-Enabled Polysulfide Entrapment. To test the hypothesis in Figure 1, $Li_2S@TiS_2$ particles were synthesized by converting 20% of the Li_2S on the surface into TiS_2 via an ion exchange process (see Supporting Information). The schematic and details of the synthesis process are shown in Supporting Information Figure S2. A scanning electron microscopy (SEM) image of Li_2S after TiS_2 coating reveals that the typical particle size of as-prepared $Li_2S@TiS_2$ ranges between 1 and 5 μm with an average size of 2 μm (Figure 2a). A transmission electron microscopy (TEM) image shows that Li_2S is encapsulated by a uniform polycrystalline TiS_2 layer with a thickness of ∼20 nm (Figure 2b). A high-resolution TEM image shows a spacing of 0.57 nm, which is consistent with the interlayer spacing of TiS_2,[47] verifying the crystalline structure of the TiS_2 layer (Figure 2c). Elemental mapping of the composite particle suggests the uniform coating of TiS_2 on the Li_2S surface (Supporting Information Figure S3). The $Li_2S@TiS_2$ particles were mixed with a carbon black conductive additive, lithium bis(trifluoromethanesulfonyl)imide (LiTFSI), and PEO binder (60:15:10:15 by weight) in acetonitrile to form a slurry, which was coated onto aluminum foils and dried in a glovebox to prepare the working electrodes. A homemade in situ optical cell (Figure 2d) was then fabricated using lithium metal as the counter electrode and PEO/LiTFSI as the electrolytes to study the dissolution behavior of intermediate polysulfides (Li_2S_x, $3 \leq x \leq 8$) in solid-polymer-based ASSLSBs. All of the components were sealed between a glass substrate and a piece of transparent cover glass slide to enable in situ optical observation and heated at 60 °C (Figure 2e). A photograph of the experimental setup is shown in Supporting Information Figure S4. Bare Li_2S was also applied as a working electrode to fabricate an optical cell for comparison.

The optical cell is first charged to a cutoff voltage of 3.8 V (versus Li^+/Li) under a current of 5 μA and then discharged to a cutoff voltage of 1.6 V under a current of −2 μA. During the charging process, the Li_2S is oxidized to polysulfides. Figure 2f,g shows the evolution of the interface between the working electrode and the solid-state PEO/LiTFSI electrolyte during

https://dx.doi.org/10.1021/acs.nanolett.0c02033
Nano Lett. XXXX, XXX, XXX−XXX

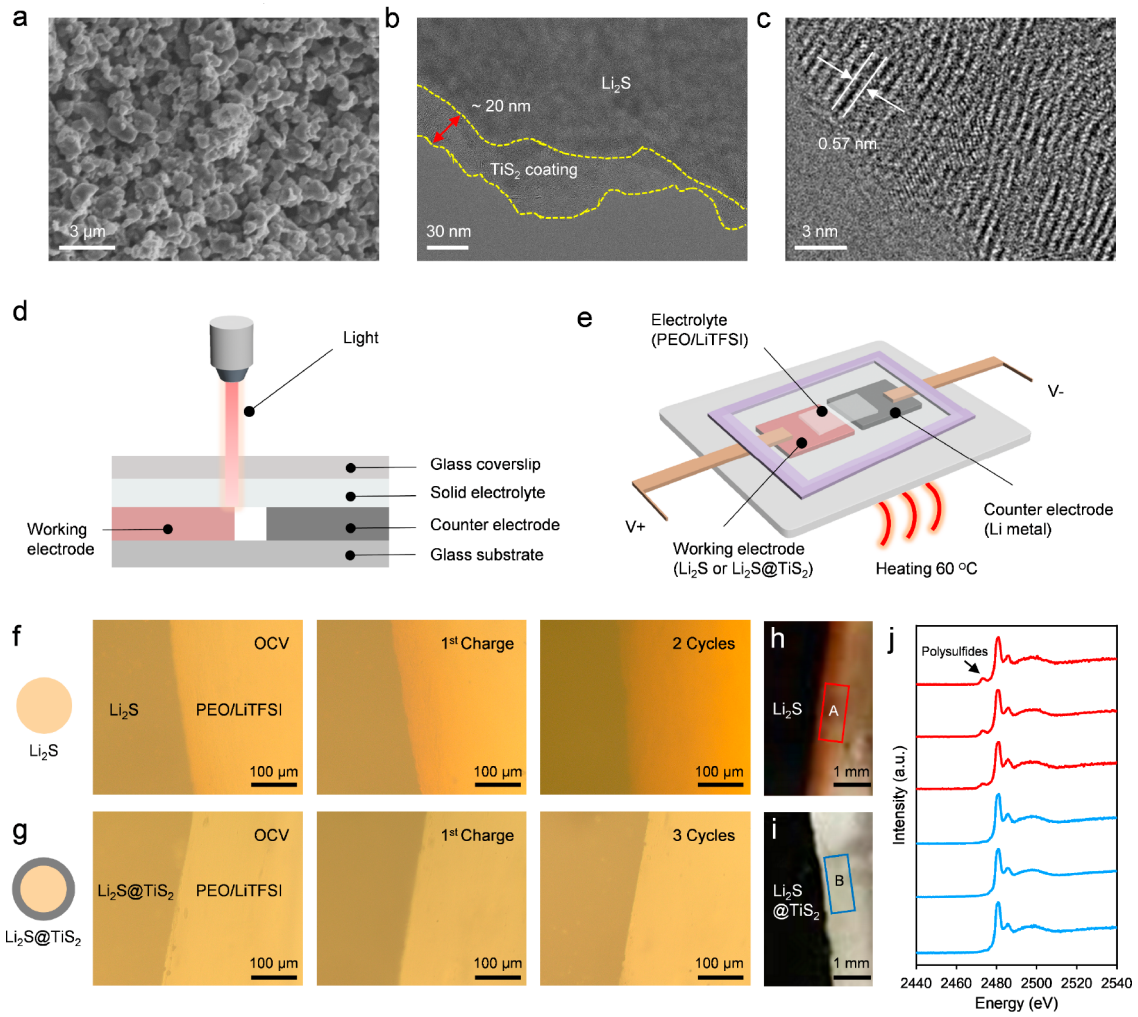

Figure 2. Polysulfides entrapment in $Li_2S@TiS_2$ cathodes. (a) SEM and (b) TEM image of $Li_2S@TiS_2$ particles. The thickness of the TiS_2 coating is approximately 20 nm. (c) High-resolution TEM image of TiS_2 coating on Li_2S. (d) Schematic of the setup for in situ optical observation. A thin gap (1−2 mm) between the working electrode and the counter electrode was designed to avoid short-circuiting. (e) Illustration of the electrochemical cell assembled with a bare Li_2S working electrode or $Li_2S@TiS_2$ working electrodes, PEO/LiTFSI electrolyte, and a lithium metal counter electrode. The entire cell is heated to 60 °C. The open-circuit voltage of the as-prepared cell is 2.5 V. The cell is first charged to 3.8 V at a constant current of 5 μA and then discharged to 1.6 V at a current of −2 μA. The in situ optical microscopy image shows the working electrode/electrolyte interface for (f) bare Li_2S electrode and (g) $Li_2S@TiS_2$ electrode. Photographs show the overall working electrode/electrolyte interface after cycling for optical cells with (h) bare Li_2S electrode and (i) $Li_2S@TiS_2$ electrode. For the optical cell with bare Li_2S working electrode, the color of the solid electrolyte near the working electrode side changes from transparent to red−brown after cycling, indicating that polysulfides are dissolving into the PEO/LiTFSI electrolyte. For the optical cell with $Li_2S@TiS_2$ working electrode, no color change is observed, indicating that polysulfides are well-trapped. (j) Sulfur K-edge X-ray absorption near-edge structure spectra of PEO/LiTFSI electrolytes in corresponding area A for bare Li_2S and area B for $Li_2S@TiS_2$ electrode. The presence of a broadened absorption peak around 2472 eV in area A confirmed the generation of polysulfides in PEO/LiTFSI electrolytes for the bare Li_2S electrode. The absorption features at 2481 and 2486 eV are from LiTFSI in the electrolyte.

the cycling process. Before being charged, the interface can be clearly observed and the pure PEO/LiTFSI electrolyte part has a pale yellow color by optical microscopy (OM) imaging at open-circuit voltage. For optical cells with bare Li_2S electrodes, only after the first charging process, the color of the PEO/LiTFSI electrolyte gradually changes from a pale-yellow color to red-brown, starting from the interface between the working electrode and the electrolyte. The red-brown coloration fully spreads over the whole PEO/LiTFSI electrolyte after only two cycles, suggesting that polysulfides are dissolving into the PEO/LiTFSI electrolyte (Figure 2f). In contrast, no obvious color change of the PEO/LiTFSI electrolyte is observed in optical cells with $Li_2S@TiS_2$ electrodes after three cycles (Figure 2g). This phenomenon is further demonstrated by the photograph of the overall working electrode/electrolyte interface. The solid-state electrolyte near the working electrode interface changes from transparent to red-brown for the bare Li_2S electrode (Figure 2h), while maintaining its original color for the $Li_2S@TiS_2$ optical cell (Figure 2i).

To further verify the composition of PEO/LiTFSI solid electrolytes after cycling, we measured sulfur K-edge X-ray absorption near-edge structure (XANES) for PEO/LiTFSI electrolytes in the corresponding area marked as A in Figure 2j for bare Li_2S and area marked as B in Figure 2j for $Li_2S@TiS_2$ electrodes. Both bare Li_2S and $Li_2S@TiS_2$ electrodes show absorption features at 2481 and 2486 eV, originating from LiTFSI in the electrolyte.[48] The presence of a broadened peak around 2472 eV in area A confirms the generation of

https://dx.doi.org/10.1021/acs.nanolett.0c02033
Nano Lett. XXXX, XXX, XXX−XXX

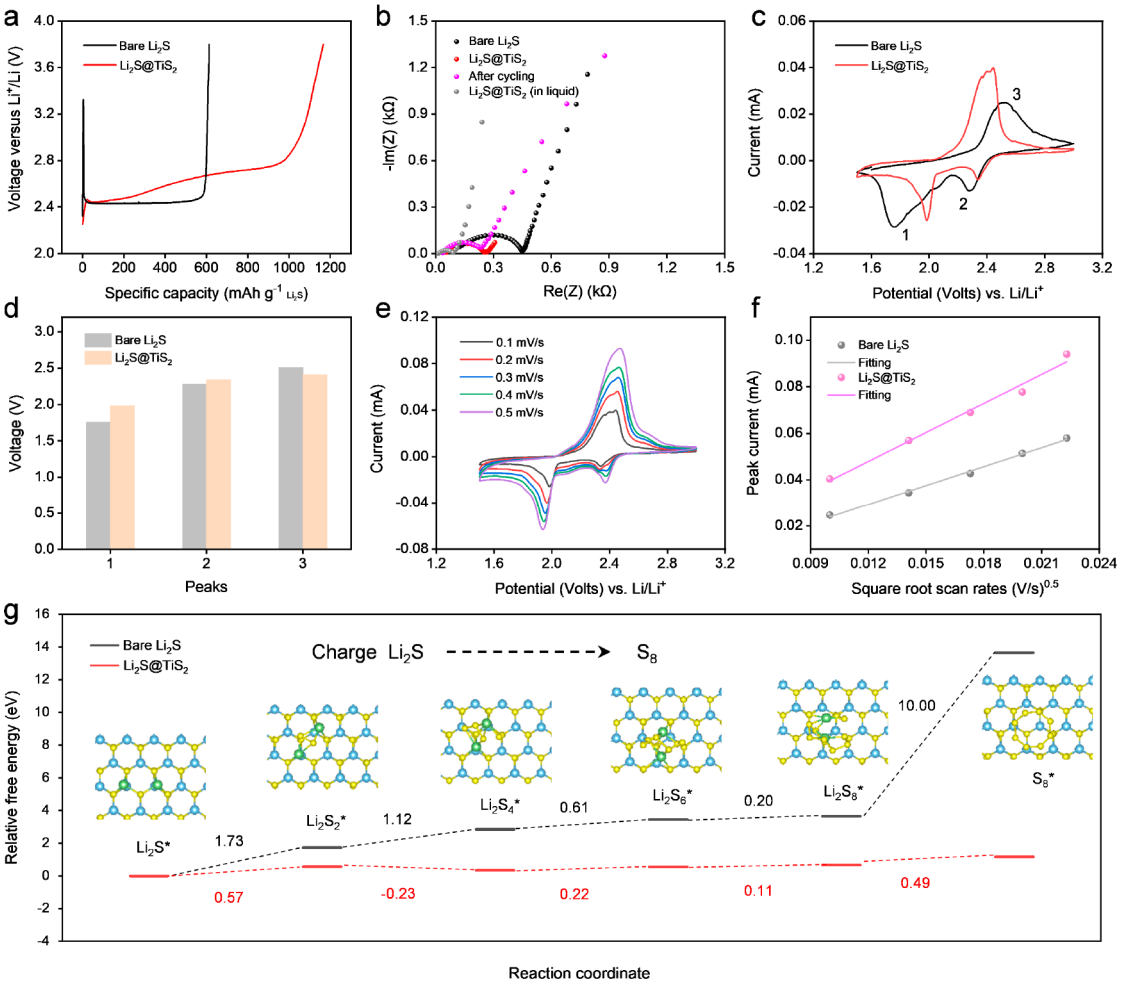

Figure 3. Electrochemical activation and electrochemical reactions in all-solid-state Li_2S–Li batteries. (a) First cycle charge voltage profiles of $Li_2S@TiS_2$ and bare Li_2S cathodes at 0.1 C (1 C = 1166 mA·g^{-1} Li_2S). (b) Electrochemical impedance spectra of ASSLSBs using bare Li_2S and $Li_2S@TiS_2$ cathodes and the liquid system data adapted from ref 13. (c) CV curves and (d) corresponding peak potentials of $Li_2S@TiS_2$ and bare Li_2S electrode. (e) CV curves of the $Li_2S@TiS_2$ electrode at various scan rates (0.1, 0.2, 0.3, 0.4, and 0.5 mV s^{-1}). (f) Plots of the CV peak current for the anodic oxidation process (peak 3: $Li_2S \rightarrow S_8$) versus the square root of the scan rates. All cells were tested at 60 °C. (g) Energy profiles for the oxidation of bare Li_2S and Li_2S on TiS_2. The optimized geometries of TiS_2 with adsorbates (Li_2S*, Li_2S_2*, Li_2S_4*, Li_2S_6*, Li_2S_8*, and S_8*) are shown in the inset (Ti, blue; S, yellow; Li, green).

polysulfides[49] in the PEO/LiTFSI electrolyte in the cell with the bare Li_2S electrode. The polysulfide dissolution in SPEs has been previously observed by SEM, ultraviolet–visible spectroscopy, and Raman spectroscopy techniques.[36,38] Here, for the first time, we report the sulfur K-edge XANES of polysulfides in SPEs to prove polysulfide dissolution. Combining in situ optical microscopy and sulfur K-edge XANES measurement, we conclude that polysulfides form and dissolve into PEO/LiTFSI electrolytes from bare Li_2S electrodes during cycling, whereas $Li_2S@TiS_2$ electrodes can effectively trap polysulfides by a structurally intact encapsulation layer, thereby avoiding polysulfide dissolution into SPEs.

TiS_2-Enhanced Li_2S Oxidation Reaction Kinetics. In addition to the function of trapping polysulfides, we would like to study whether TiS_2 coating could play a crucial role in promoting Li_2S oxidation kinetics in solid-state electrolytes, as this was proven in liquid electrolytes.[46] Coin cells (type 2032) are assembled using Li_2S composite cathodes, PI@PEO/LiTFSI electrolytes, and lithium metal anodes. Due to the large charge transfer resistance and intrinsically poor electronic conductivity of Li_2S,[45] the as-assembled unencapsulated Li_2S cells show a high energy barrier of 3.3 V at the initial charge cycle for activation (Figure 3a) at a rate of 0.1 C and a large charge transfer resistance at open-circuit voltage (Figure 3b). It indicates that the oxidation reaction may only occur at the localized regions of the active particles directly interfacing electron and ion transfer channels, thus resulting in a much lower specific capacity than the theoretical value. After TiS_2 coating, the initial activation energy barrier significantly decreases below 2.5 V (Figure 3a). This is direct evidence that the TiS_2 coating facilitates Li_2S oxidation reaction. Moreover, owing to the high conductivity of TiS_2, the impedance spectrum of the as-assembled $Li_2S@TiS_2$ cells also shows a smaller semicircle in the high-frequency region compared with bare Li_2S cells, indicating a reduced charge transfer resistance (Figure 3b). The charge transfer resistance is comparable with that in the liquid system and further decreases after 10 cycles, which indicates the formation of a stable TiS_2 interface, allowing fast charge transfer during cycling.

Cyclic voltammetry (CV) evaluation on the as-assembled cells provides additional evidence for the catalytic effect of TiS_2

https://dx.doi.org/10.1021/acs.nanolett.0c02033
Nano Lett. XXXX, XXX, XXX–XXX

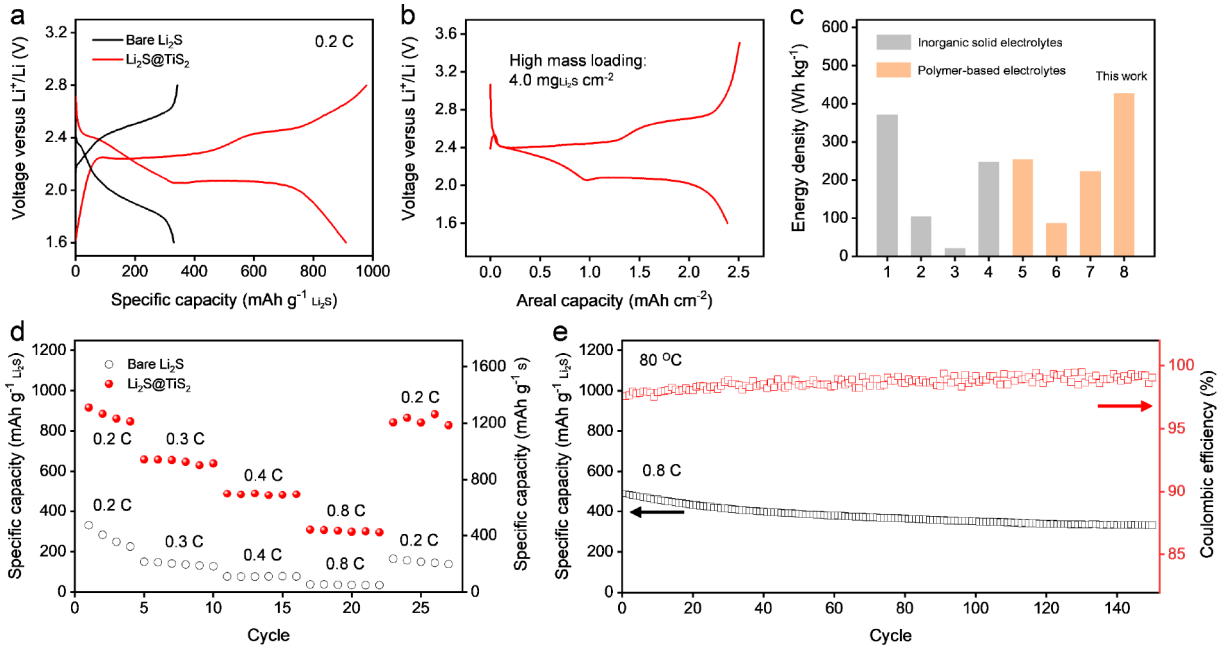

Figure 4. Electrochemical performance of $Li_2S@TiS_2$ cathodes and bare Li_2S cathodes in ASSLSBs. (a) Charge−discharge voltage profiles of $Li_2S@TiS_2$ and bare Li_2S cathodes at 0.2 C at 60 °C. (b) Voltage profile and areal capacity of $Li_2S@TiS_2$ cathode with a high mass loading (4.0 mg·cm^{-2}) at a current density of 0.04 mA·cm^{-2} at 60 °C. (c) Energy density chart of ASSLSBs. The numbers in the horizontal axis correspond to the entries listed in Supporting Information Table S1. (d) Rate performance of $Li_2S@TiS_2$ and bare Li_2S cathodes at various charging rates, cycled at 60 °C, within a potential window of 1.6−2.8 V versus Li^+/Li. (e) Cycling performance and Coulombic efficiency of the $Li_2S@TiS_2$ cathode at 0.8 C for 150 cycles at 80 °C. Ultrathin Li metal foils (~40 μm) are used as the counter electrodes.

in ASSLSBs. Figure 3c shows distinct redox peaks for both the $Li_2S@TiS_2$ electrode and the bare Li_2S electrode. The anodic oxidation reaction (peak 3) corresponds to the oxidation of Li_2S to S_8.[46] The two reduction peaks (peaks 1 and 2) can be associated with the reduction of S_8 to long-chain lithium polysulfides and then transforms to short-chain Li_2S_2/Li_2S, respectively.[46] When compared to bare Li_2S electrodes, the $Li_2S@TiS_2$ electrodes demonstrate a lower oxidation potential and higher reduction potential (Figure 3d), suggesting that the TiS_2 coating significantly reduces the electrode polarization by catalyzing Li−S redox reactions in ASSLSBs.

Additionally, the CV curves of as-prepared electrodes at various scan rates are used to study the electrode kinetics with respect to the lithium-ion diffusion coefficient, as shown in Figure 3e and Supporting Information Figure S5. The CV peak current versus the square root of the scan rates for both $Li_2S@TiS_2$ and Li_2S electrodes (Figure 3f) shows a linear relationship. Notably, the slope of the $Li_2S@TiS_2$ curve is larger than that of the bare Li_2S. According to the classical Randles−Sevcik equation for a diffusion-limited process,[46,50] a larger slope of the curve for the $Li_2S@TiS_2$ electrode indicates a faster lithium diffusion within the $Li_2S@TiS_2$ electrode compared to that with the bare Li_2S electrode, which further facilitates sulfur transformation reactions.

To attain an in-depth understanding of the catalytic effect of TiS_2 coating for improved charge reaction kinetics in ASSLSBs, the overall reaction mechanism for Li_2S oxidation is simulated theoretically, as shown in Figure 3g. First-principles calculations propose detailed energetics and kinetics of reaction steps for the TiS_2-modulated Li_2S oxidation. The optimized geometries of TiS_2 with adsorbates are shown in the inset, whereas the atomic configurations of bare Li_2S reaction coordinates can be seen in Supporting Information Figure S6. For each reaction step, the energy barriers of $Li_2S@TiS_2$ are much lower than those of the bare Li_2S, as shown in Figure 3g. Two steps from Li_2S to Li_2S_2 and Li_2S_8 to S_8 exhibit the two largest positive Gibbs energy barriers among all of the steps. The energy barrier of Li_2S to Li_2S_2 of TiS_2-modulated Li_2S oxidation is 0.57 eV, which is significantly lower than that of bare Li_2S oxidation, 1.73 eV. This correlates very well with the experimental evidence that the energy barrier of $Li_2S@TiS_2$ is significantly reduced (Figure 3a). Moreover, we note that the rate-limiting step for the bare Li_2S is the step from Li_2S_8 to the S_8 with a value of 10.00 eV, whereas the value of $Li_2S@TiS_2$ is only 0.49 eV. As a result, TiS_2-modulated Li_2S oxidation becomes the fast and energetically favored reaction, which results in the enhanced electrochemical performance of Li−S batteries.

Electrochemical Performance of $Li_2S@TiS_2$ Cathodes in All-Solid-State Li−S Batteries. We further prove the efficacy of nanoscale encapsulation in the solid-state system by testing the electrochemical performance of $Li_2S@TiS_2$ cathodes in lithium metal batteries (type 2032) with SPEs. Cross-sectional SEM images of the typical cell are shown in Supporting Information Figure S7. As-assembled cells are constructed for galvanostatic cycling tests from 1.6 to 2.8 V. A specific capacity as high as ~910 mAh·g^{-1} Li_2S at 0.2 C (1 C = 1166 mA·g^{-1} Li_2S) is realized by $Li_2S@TiS_2$ cathodes, which is more than 2 times higher than that of the bare Li_2S one (~330 mAh·g^{-1}) (Figure 4a). Additionally, the $Li_2S@TiS_2$ cathode with a high mass loading of Li_2S is fabricated and tested in ASSLSBs, obtaining an areal capacity of 2.4 mA·h·cm^{-2} at 60 °C (Figure 4b), which corresponds to a high cell-level energy density of 427 W·h·kg^{-1}. The energy density is calculated from the average discharge voltage (2.1 V), cell capacity (2.4 mA·h·cm^{-2}), and total mass of the cathode (8.6 mg·cm^{-2}, excluding current collector), the solid electrolyte (1.2 mg·cm^{-2}), and the anode (2.0 mg·cm^{-2}). The energy density of our work

https://dx.doi.org/10.1021/acs.nanolett.0c02033
Nano Lett. XXXX, XXX, XXX−XXX

outperforms most previously reported ASSLSBs[21,22,31,40,51−53] (Figure 4c and Supporting Information Table S1).

In addition, the rate performance of as-prepared cathodes is investigated by cycling cells at different C-rates (Figure 4d). For the bare Li_2S cathode, significant capacity fading (from 330 to 226 mAh·g^{-1}) is observed during four cycles at 0.2 C, with capacity severely decreasing to 38.5 mAh·g^{-1} at a higher rate of 0.8 C. Comparatively, the Li_2S@TiS_2 cell, benefiting from the effective TiS_2-enhanced oxidation kinetics, shows a much better rate capability, achieving a discharge capacity of 660, 488, and 309 mAh·g^{-1} based on Li_2S at 0.3, 0.4, and 0.8 C, respectively. Moreover, the Li_2S@TiS_2 cell exhibits stable cycling performance after charge/discharge cycling at 0.8 C at 60 and 80 °C, as shown in Supporting Information Figure S8 and Figure 4e. After an initial discharge capacity of 490 mAh·g^{-1} at 80 °C, the Li_2S@TiS_2 cells retain 79, 71, and 68% of their initial capacity after 50, 100, and 150 cycles, respectively (Figure 4e). Average Coulombic efficiency after 150 cycles is calculated to be 98.6%, which shows little shuttle effect owing to efficient polysulfide trapping by TiS_2 encapsulation. We disassemble the Li_2S@TiS_2 cell after 150 cycles and find the PI@PEO/LiTFSI electrolyte in the Li_2S@TiS_2 cell maintains its original color (Figure S9), which further proves the efficacy of nanoscale encapsulation. All of the above results show that TiS_2 encapsulation enables polysulfide entrapment and enhances oxidation kinetics to achieve high-performance ASSLSBs.

In summary, the concept of nanoscale encapsulation from liquid Li−S batteries has been successfully proven to be effective in solid-state batteries, as well. As an example, the Li_2S@TiS_2 cathode is fabricated by a facile in situ reaction, which enables polysulfide entrapment and promotes Li_2S oxidation. Combining the cathode with ultrathin PI@PEO/LiTFSI electrolyte (10−20 μm) and lithium metal anode, a high cell-level energy density (excluding the current collectors) of 427 W·h·kg^{-1} is achieved with a high mass loading of 4.0 mg·cm^{-2}. Through in situ optical microscopy and sulfur K-edge XANES measurements, we have demonstrated that TiS_2 coating successfully traps polysulfides in the cathode, thus achieving high energy density ASSLSBs. These studies will provide useful insights into the fundamental understanding of Li−S conversion chemistry in SPEs and advanced electrode design for next-generation high-performance and safe ASSLSBs.

■ ASSOCIATED CONTENT

Supporting Information

The Supporting Information is available free of charge at https://pubs.acs.org/doi/10.1021/acs.nanolett.0c02033.

Experimental details, characterization methods, and supplementary figures (PDF)

■ AUTHOR INFORMATION

Corresponding Author

Yi Cui − *Department of Materials Science and Engineering, Stanford University, Stanford, California 94305, United States; Stanford Institute for Materials and Energy Sciences, SLAC National Accelerator Laboratory, Menlo Park, California 94025, United States;* orcid.org/0000-0002-6103-6352; Email: yicui@stanford.edu

Authors

Xin Gao − *Department of Materials Science and Engineering, Stanford University, Stanford, California 94305, United States;* orcid.org/0000-0001-5360-0796

Xueli Zheng − *Department of Materials Science and Engineering, Stanford University, Stanford, California 94305, United States;* orcid.org/0000-0002-6800-2649

Jingyang Wang − *Department of Materials Science and Engineering, Stanford University, Stanford, California 94305, United States; Materials Sciences Division, Lawrence Berkeley National Laboratory, Berkeley, California 94720, United States*

Zewen Zhang − *Department of Materials Science and Engineering, Stanford University, Stanford, California 94305, United States;* orcid.org/0000-0002-4909-4330

Xin Xiao − *Department of Materials Science and Engineering, Stanford University, Stanford, California 94305, United States;* orcid.org/0000-0003-1098-9484

Jiayu Wan − *Department of Materials Science and Engineering, Stanford University, Stanford, California 94305, United States;* orcid.org/0000-0003-4778-1732

Yusheng Ye − *Department of Materials Science and Engineering, Stanford University, Stanford, California 94305, United States;* orcid.org/0000-0001-9832-2478

Lien-Yang Chou − *Department of Materials Science and Engineering, Stanford University, Stanford, California 94305, United States*

Hiang Kwee Lee − *Department of Materials Science and Engineering, Stanford University, Stanford, California 94305, United States*

Jiangyan Wang − *Department of Materials Science and Engineering, Stanford University, Stanford, California 94305, United States;* orcid.org/0000-0001-6951-1296

Rafael A. Vilá − *Department of Materials Science and Engineering, Stanford University, Stanford, California 94305, United States*

Yufei Yang − *Department of Materials Science and Engineering, Stanford University, Stanford, California 94305, United States*

Pu Zhang − *Department of Materials Science and Engineering, Stanford University, Stanford, California 94305, United States*

Lin-Wang Wang − *Materials Sciences Division, Lawrence Berkeley National Laboratory, Berkeley, California 94720, United States*

Complete contact information is available at: https://pubs.acs.org/10.1021/acs.nanolett.0c02033

Author Contributions

Y.C. and X.G. conceived the concept and experiments. X.G. performed material preparation and electrochemical measurements. X.G. and X.Z. carried out in situ optical cell fabrication and imaging. J.W. and L.W. performed DFT calculation. Z.Z. and R.A.V. performed TEM characterizations. X.X. performed SEM characterizations. X.Z. performed XAS measurements. J.W., Y.Y., L.C., H.K.L., Y.Y., and P.Z. assisted in material preparation and characterizations. J.W. and Y.Y. assisted in electrochemical measurements. All authors contributed to data discussions. X.G. and Y.C. analyzed data and wrote the paper with input from all authors.

Notes

The authors declare no competing financial interest.

https://dx.doi.org/10.1021/acs.nanolett.0c02033
Nano Lett. XXXX, XXX, XXX−XXX

■ ACKNOWLEDGMENTS

Y.C. acknowledges the support from the Assistant Secretary for Energy Efficiency and Renewable Energy, Office of Vehicle Technologies, of the U.S. Department of Energy under the Battery Materials Research (BMR) Program and the Battery500 Consortium program. R.A.V. acknowledges support from the National Academy of Sciences Ford Foundation Fellowship and the National Science Foundation Graduate Research Fellowship Program (NSF GRFP, Grant No. DGE-1656518). We acknowledge Dr. Sirine Fakra from Advanced Light Source for X-ray absorption measurements. X.G. acknowledges Yuchi Tsao, Dr. Fang Liu, and Dr. Guangmin Zhou for helpful discussions.

■ REFERENCES

(1) Armand, M.; Tarascon, J. M. Building better batteries. *Nature* **2008**, *451* (7), 652−657.
(2) Bruce, P. G.; Freunberger, S. A.; Hardwick, L. J.; Tarascon, J. M. Li-O_2 and Li-S batteries with high energy storage. *Nat. Mater.* **2012**, *11* (1), 19−29.
(3) Cano, Z. P.; Banham, D.; Ye, S.; Hintennach, A.; Lu, J.; Fowler, M.; Chen, Z. Batteries and fuel cells for emerging electric vehicle markets. *Nat. Energy* **2018**, *3* (4), 279−289.
(4) Evers, S.; Nazar, L. F. New Approaches for High Energy Density Lithium-Sulfur Battery Cathodes. *Acc. Chem. Res.* **2013**, *46* (5), 1135−1143.
(5) Pang, Q.; Liang, X.; Kwok, C. Y.; Nazar, L. F. Advances in lithium-sulfur batteries based on multifunctional cathodes and electrolytes. *Nat. Energy* **2016**, *1* (9), 1−11.
(6) Zheng, G.; Zhang, Q.; Cha, J. J.; Yang, Y.; Li, W.; Seh, Z. W.; Cui, Y. Amphiphilic surface modification of hollow carbon nanofibers for improved cycle life of lithium sulfur batteries. *Nano Lett.* **2013**, *13* (3), 1265−70.
(7) Liu, Y.; He, P.; Zhou, H. Rechargeable Solid-State Li-Air and Li-S Batteries: Materials, Construction, and Challenges. *Adv. Energy Mater.* **2018**, *8* (4), 1701602.
(8) Xu, R.; Lu, J.; Amine, K. Progress in Mechanistic Understanding and Characterization Techniques of Li-S Batteries. *Adv. Energy Mater.* **2015**, *5* (16), 1500408.
(9) Seh, Z. W.; Sun, Y.; Zhang, Q.; Cui, Y. Designing high-energy lithium-sulfur batteries. *Chem. Soc. Rev.* **2016**, *45* (20), 5605−5634.
(10) Ji, X.; Lee, K. T.; Nazar, L. F. A highly ordered nanostructured carbon-sulphur cathode for lithium-sulphur batteries. *Nat. Mater.* **2009**, *8* (6), 500−506.
(11) Li, Z.; Wu, H. B.; Lou, X. W. Rational designs and engineering of hollow micro-/nanostructures as sulfur hosts for advanced lithium-sulfur batteries. *Energy Environ. Sci.* **2016**, *9* (10), 3061−3070.
(12) Seh, Z. W.; Li, W.; Cha, J. J.; Zheng, G.; Yang, Y.; McDowell, M. T.; Hsu, P.-C.; Cui, Y. Sulphur-TiO_2 yolk-shell nanoarchitecture with internal void space for long-cycle lithium-sulphur batteries. *Nat. Commun.* **2013**, *4* (1), 1331.
(13) Seh, Z. W.; Yu, J. H.; Li, W.; Hsu, P. C.; Wang, H.; Sun, Y.; Yao, H.; Zhang, Q.; Cui, Y. Two-dimensional layered transition metal disulphides for effective encapsulation of high-capacity lithium sulphide cathodes. *Nat. Commun.* **2014**, *5* (1), 5017.
(14) Bai, S.; Liu, X.; Zhu, K.; Wu, S.; Zhou, H. Metal-organic framework-based separator for lithium-sulfur batteries. *Nat. Energy* **2016**, *1* (7), 16094.
(15) Jeong, Y. C.; Kim, J. H.; Nam, S.; Park, C. R.; Yang, S. J. Rational Design of Nanostructured Functional Interlayer/Separator for Advanced Li-S Batteries. *Adv. Funct. Mater.* **2018**, *28* (38), 1707411.
(16) Li, G.; Gao, Y.; He, X.; Huang, Q.; Chen, S.; Kim, S. H.; Wang, D. Organosulfide-plasticized solid-electrolyte interphase layer enables stable lithium metal anodes for long-cycle lithium-sulfur batteries. *Nat. Commun.* **2017**, *8* (1), 850.
(17) Janek, J.; Zeier, W. G. A solid future for battery development. *Nat. Energy* **2016**, *1* (9), 16141.
(18) Hassoun, J.; Scrosati, B. Moving to a solid-state configuration: a valid approach to making lithium-sulfur batteries viable for practical applications. *Adv. Mater.* **2010**, *22* (45), 5198−5201.
(19) Li, W.; Wang, Q.; Jin, J.; Li, Y.; Wu, M.; Wen, Z. Constructing dual interfacial modification by synergetic electronic and ionic conductors: Toward high-performance LAGP-Based Li-S batteries. *Energy Storage Mater.* **2019**, *23*, 299−305.
(20) Gu, S.; Huang, X.; Wang, Q.; Jin, J.; Wang, Q.; Wen, Z.; Qian, R. A hybrid electrolyte for long-life semi-solid-state lithium sulfur batteries. *J. Mater. Chem. A* **2017**, *5* (27), 13971−13975.
(21) Xu, R.; Yue, J.; Liu, S.; Tu, J.; Han, F.; Liu, P.; Wang, C. Cathode-Supported All-Solid-State Lithium-Sulfur Batteries with High Cell-Level Energy Density. *ACS Energy Lett.* **2019**, *4* (5), 1073−1079.
(22) Yan, H.; Wang, H.; Wang, D.; Li, X.; Gong, Z.; Yang, Y. In Situ Generated Li_2S-C Nanocomposite for High-Capacity and Long-Life All-Solid-State Lithium Sulfur Batteries with Ultrahigh Areal Mass Loading. *Nano Lett.* **2019**, *19* (5), 3280−3287.
(23) Nagao, M.; Hayashi, A.; Tatsumisago, M. High-capacity Li_2S-nanocarbon composite electrode for all-solid-state rechargeable lithium batteries. *J. Mater. Chem.* **2012**, *22* (19), 10015−10020.
(24) Kato, Y.; Hori, S.; Saito, T.; Suzuki, K.; Hirayama, M.; Mitsui, A.; Yonemura, M.; Iba, H.; Kanno, R. High-power all-solid-state batteries using sulfide superionic conductors. *Nat. Energy* **2016**, *1* (4), 16030.
(25) Wenzel, S.; Weber, D. A.; Leichtweiss, T.; Busche, M. R.; Sann, J.; Janek, J. Interphase formation and degradation of charge transfer kinetics between a lithium metal anode and highly crystalline Li7P3S11 solid electrolyte. *Solid State Ionics* **2016**, *286*, 24−33.
(26) Wang, Y.; Lu, D.; Bowden, M.; El Khoury, P. Z.; Han, K. S.; Deng, Z. D.; Xiao, J.; Zhang, J.-G.; Liu, J. Mechanism of Formation of $Li_7P_3S_{11}$ Solid Electrolytes through Liquid Phase Synthesis. *Chem. Mater.* **2018**, *30* (3), 990−997.
(27) Zheng, Q.; Ma, L.; Khurana, R.; Archer, L. A.; Coates, G. W. Structure-property study of cross-linked hydrocarbon/poly(ethylene oxide) electrolytes with superior conductivity and dendrite resistance. *Chem. Sci.* **2016**, *7* (11), 6832−6838.
(28) Xu, K. Electrolytes and interphases in Li-ion batteries and beyond. *Chem. Rev.* **2014**, *114* (23), 11503−11618.
(29) Lin, D.; Liu, W.; Liu, Y.; Lee, H. R.; Hsu, P. C.; Liu, K.; Cui, Y. High Ionic Conductivity of Composite Solid Polymer Electrolyte via In Situ Synthesis of Monodispersed SiO_2 Nanospheres in Poly(ethylene oxide). *Nano Lett.* **2016**, *16* (1), 459−465.
(30) Croce, F.; Appetecchi, G. B.; Persi, L.; Scrosati, B. Nanocomposite polymer electrolytes for lithium batteries. *Nature* **1998**, *394* (6692), 456−458.
(31) Tao, X.; Liu, Y.; Liu, W.; Zhou, G.; Zhao, J.; Lin, D.; Zu, C.; Sheng, O.; Zhang, W.; Lee, H. W.; Cui, Y. Solid-State Lithium-Sulfur Batteries Operated at 37 degrees C with Composites of Nanostructured Li7La3Zr2O12/Carbon Foam and Polymer. *Nano Lett.* **2017**, *17* (5), 2967−2972.
(32) Judez, X.; Zhang, H.; Li, C.; Eshetu, G. G.; Zhang, Y.; Gonzalez-Marcos, J. A.; Armand, M.; Rodriguez-Martinez, L. M. Polymer-Rich Composite Electrolytes for All-Solid-State Li-S Cells. *J. Phys. Chem. Lett.* **2017**, *8* (15), 3473−3477.
(33) Wan, J.; Xie, J.; Kong, X.; Liu, Z.; Liu, K.; Shi, F.; Pei, A.; Chen, H.; Chen, W.; Chen, J.; Zhang, X.; Zong, L.; Wang, J.; Chen, L. Q.; Qin, J.; Cui, Y. Ultrathin, flexible, solid polymer composite electrolyte enabled with aligned nanoporous host for lithium batteries. *Nat. Nanotechnol.* **2019**, *14* (7), 705−711.
(34) Cui, Y.; Wan, J.; Ye, Y.; Liu, K.; Chou, L. Y.; Cui, Y. A Fireproof, Lightweight, Polymer-Polymer Solid-State Electrolyte for Safe Lithium Batteries. *Nano Lett.* **2020**, *20* (3), 1686−1692.
(35) Nie, K.; Wang, X.; Qiu, J.; Wang, Y.; Yang, Q.; Xu, J.; Yu, X.; Li, H.; Huang, X.; Chen, L. Increasing Poly(ethylene oxide) Stability to 4.5 V by Surface Coating of the Cathode. *ACS Energy Lett.* **2020**, *5* (3), 826−832.

https://dx.doi.org/10.1021/acs.nanolett.0c02033
Nano Lett. XXXX, XXX, XXX−XXX

(36) Song, Y.-X.; Shi, Y.; Wan, J.; Lang, S.-Y.; Hu, X.-C.; Yan, H.-J.; Liu, B.; Guo, Y.-G.; Wen, R.; Wan, L.-J. Direct tracking of the polysulfide shuttling and interfacial evolution in all-solid-state lithium-sulfur batteries: a degradation mechanism study. *Energy Environ. Sci.* **2019**, *12* (8), 2496−2506.
(37) Yang, X.; Luo, J.; Sun, X. Towards high-performance solid-state Li-S batteries: from fundamental understanding to engineering design. *Chem. Soc. Rev.* **2020**, *49* (7), 2140−2195.
(38) Marceau, H.; Kim, C.-S.; Paolella, A.; Ladouceur, S.; Lagacé, M.; Chaker, M.; Vijh, A.; Guerfi, A.; Julien, C. M.; Mauger, A.; Armand, M.; Hovington, P.; Zaghib, K. In operando scanning electron microscopy and ultraviolet-visible spectroscopy studies of lithium/sulfur cells using all solid-state polymer electrolyte. *J. Power Sources* **2016**, *319*, 247−254.
(39) Liang, X.; Wen, Z.; Liu, Y.; Zhang, H.; Huang, L.; Jin, J. Highly dispersed sulfur in ordered mesoporous carbon sphere as a composite cathode for rechargeable polymer Li/S battery. *J. Power Sources* **2011**, *196* (7), 3655−3658.
(40) Zhang, H.; Oteo, U.; Judez, X.; Eshetu, G. G.; Martinez-Ibañez, M.; Carrasco, J.; Li, C.; Armand, M. Designer Anion Enabling Solid-State Lithium-Sulfur Batteries. *Joule* **2019**, *3* (7), 1689−1702.
(41) Eshetu, G. G.; Judez, X.; Li, C.; Martinez-Ibanez, M.; Gracia, I.; Bondarchuk, O.; Carrasco, J.; Rodriguez-Martinez, L. M.; Zhang, H.; Armand, M. Ultrahigh Performance All Solid-State Lithium Sulfur Batteries: Salt Anion's Chemistry-Induced Anomalous Synergistic Effect. *J. Am. Chem. Soc.* **2018**, *140* (31), 9921−9933.
(42) Eshetu, G. G.; Judez, X.; Li, C.; Bondarchuk, O.; Rodriguez-Martinez, L. M.; Zhang, H.; Armand, M. Lithium Azide as an Electrolyte Additive for All-Solid-State Lithium-Sulfur Batteries. *Angew. Chem., Int. Ed.* **2017**, *56* (48), 15368−15372.
(43) Jiang, J.; Zhu, J.; Ai, W.; Wang, X.; Wang, Y.; Zou, C.; Huang, W.; Yu, T. Encapsulation of sulfur with thin-layered nickel-based hydroxides for long-cyclic lithium-sulfur cells. *Nat. Commun.* **2015**, *6* (1), 8622.
(44) Wang, X.; Li, G.; Li, J.; Zhang, Y.; Wook, A.; Yu, A.; Chen, Z. Structural and chemical synergistic encapsulation of polysulfides enables ultralong-life lithium-sulfur batteries. *Energy Environ. Sci.* **2016**, *9* (8), 2533−2538.
(45) Yang, Y.; Zheng, G.; Misra, S.; Nelson, J.; Toney, M. F.; Cui, Y. High-capacity micrometer-sized Li2S particles as cathode materials for advanced rechargeable lithium-ion batteries. *J. Am. Chem. Soc.* **2012**, *134* (37), 15387−15394.
(46) Zhou, G.; Tian, H.; Jin, Y.; Tao, X.; Liu, B.; Zhang, R.; Seh, Z. W.; Zhuo, D.; Liu, Y.; Sun, J.; Zhao, J.; Zu, C.; Wu, D. S.; Zhang, Q.; Cui, Y. Catalytic oxidation of Li_2S on the surface of metal sulfides for Li-S batteries. *Proc. Natl. Acad. Sci. U. S. A.* **2017**, *114* (5), 840−845.
(47) Chen, J.; Li, S.-L.; Tao, Z.-L.; Shen, Y.-T.; Cui, C.-X. Titanium Disulfide Nanotubes as Hydrogen-Storage Materials. *J. Am. Chem. Soc.* **2003**, *125*, 5284−5285.
(48) Yang, A.; Zhou, G.; Kong, X.; Vila, R. A.; Pei, A.; Wu, Y.; Yu, X.; Zheng, X.; Wu, C. L.; Liu, B.; Chen, H.; Xu, Y.; Chen, D.; Li, Y.; Fakra, S.; Hwang, H. Y.; Qin, J.; Chu, S.; Cui, Y. Electrochemical generation of liquid and solid sulfur on two-dimensional layered materials with distinct areal capacities. *Nat. Nanotechnol.* **2020**, *15*, 231−237.
(49) Pascal, T. A.; Wujcik, K. H.; Velasco-Velez, J.; Wu, C.; Teran, A. A.; Kapilashrami, M.; Cabana, J.; Guo, J.; Salmeron, M.; Balsara, N.; Prendergast, D. X-ray Absorption Spectra of Dissolved Polysulfides in Lithium-Sulfur Batteries from First-Principles. *J. Phys. Chem. Lett.* **2014**, *5* (9), 1547−1551.
(50) Li, P.; Shao, L.; Wang, P.; Zheng, X.; Yu, H.; Qian, S.; Shui, M.; Long, N.; Shu, J. Lithium sodium vanadium phosphate and its phase transition as cathode material for lithium ion batteries. *Electrochim. Acta* **2015**, *180*, 120−128.
(51) Han, F.; Yue, J.; Fan, X.; Gao, T.; Luo, C.; Ma, Z.; Suo, L.; Wang, C. High-Performance All-Solid-State Lithium-Sulfur Battery Enabled by a Mixed-Conductive Li_2S Nanocomposite. *Nano Lett.* **2016**, *16* (7), 4521−4527.
(52) Fu, K.; Gong, Y.; Hitz, G. T.; McOwen, D. W.; Li, Y.; Xu, S.; Wen, Y.; Zhang, L.; Wang, C.; Pastel, G.; Dai, J.; Liu, B.; Xie, H.; Yao, Y.; Wachsman, E. D.; Hu, L. Three-dimensional bilayer garnet solid electrolyte based high energy density lithium metal-sulfur batteries. *Energy Environ. Sci.* **2017**, *10* (7), 1568−1575.
(53) Judez, X.; Zhang, H.; Li, C.; Gonzalez-Marcos, J. A.; Zhou, Z.; Armand, M.; Rodriguez-Martinez, L. M. Lithium Bis(fluorosulfonyl)-imide/Poly(ethylene oxide) Polymer Electrolyte for All Solid-State Li-S Cell. *J. Phys. Chem. Lett.* **2017**, *8* (9), 1956−1960.

https://dx.doi.org/10.1021/acs.nanolett.0c02033
Nano Lett. XXXX, XXX, XXX−XXX